Mon. Not. R. Astron. Soc. **341,** 1246–1252 (2003)

Simulated X-ray cluster temperature maps

Lesley I. Onuora,★ Scott T. Kay and Peter A. Thomas
Astronomy Centre, University of Sussex, Falmer, Brighton BN1 9QJ

Accepted 2003 February 3. Received 2003 February 3; in original form 2002 September 27

ABSTRACT

Temperature maps are presented of the nine largest clusters in the mock catalogues of Muanwong et al. for both the *Preheating* and *Radiative* models. The maps show that clusters are not smooth, featureless systems, but contain a variety of substructure which should be observable. The surface brightness contours are generally elliptical and features that are seen include cold clumps, hot spiral features and cold fronts. Profiles of emission-weighted temperature, surface brightness, density and pressure across the surface brightness discontinuities seen in one of the bimodal clusters are consistent with the cold front in Abell 2142 observed by Markevitch et al.

Key words: galaxies: clusters: general – large-scale structure of Universe.

1 INTRODUCTION

X-ray surface brightness and temperature observations of clusters indicate the presence of substructure and support the view that cluster formation occurs through the infall and merger of subclusters. Studies of centroid shifts and ellipticity in clusters from both *Einstein* observations and simulations (Evrard et al. 1993; Mohr, Fabricant & Geller 1993; Mohr et al. 1995) were used as tracers of continuing dynamical evolution in clusters. Using *ROSAT* Position Sensitive Proportional Counter (PSPC) observations, Briel & Henry (1994) produced an X-ray temperature map of A2256 showing two hot regions and a low-temperature infalling subgroup. Markevitch (1996) studied the non-isothermality of the temperature distribution of the same cluster as well as three other clusters using *ASCA* data.

More recently, higher-resolution *Chandra* observations have allowed more detailed studies of the temperature structure of clusters to be performed (e.g. Markevitch et al. 2000; Forman et al. 2001). Merger shocks would be expected to occur in such a scenario (e.g. Markevitch & Vikhlinin 2001; Markevitch et al. 2002) but additionally *Chandra* observations have revealed a new phenomenon of 'cold fronts' (Markevitch et al. 2000; Forman et al. 2001; Vikhlinin, Markevitch & Murray 2001; Mazzotta, Fusco-Femiano & Vikhlinin 2002). At a cold front, the entropy jump across the sharp gas density discontinuity is in the opposite sense to that expected for a shock, with the high surface brightness side of the discontinuity corresponding to low temperature.

These features contain information on the physical processes that are occurring as well the stage, geometry, scale and velocity of the mergers. To study these processes a number of authors have carried out simulations of controlled, single mergers. Roettiger, Burns & Loken (1993), Schindler & Müller (1993) and Roettiger, Loken & Burns (1997) simulated the head-on merger of unequal-mass clusters containing gas and dark matter. For these simulations the hydrodynamics were modelled using a finite-difference code while the dark matter was modelled using an N-body particle code. Pearce, Thomas & Couchman (1994) simulated equal-mass head-on mergers using smoothed particle hydrodynamics (SPH) to follow the gas and an adaptive particle–particle, particle–mesh to handle the gravity. Using the same methods, Ritchie & Thomas (2002) carried out high-resolution simulations to study the effect on the observable properties of clusters of single head-on and off-centre mergers between both equal- and unequal-mass objects. They produced a sequence of maps of emission-weighted temperature with superimposed X-ray surface brightness and velocity fields for mergers between equal-mass systems showing the compression and shocking of the gas as the merger progressed. Takizawa (1999, 2000) carried out lower-resolution SPH simulations and Ricker & Sarazin (2001) also modelled off-centre mergers.

Recently Nagai & Kravtsov (2003) carried out a detailed study of cold fronts in high-resolution simulations of two clusters forming in different cold dark matter models (standard CDM and ΛCDM). Their results indicate that cold fronts are probably fairly common and are non-equilibrium transient phenomena. Bialek, Evrard & Mohr (2002) simulated a cluster of galaxies with a pre-heated intracluster medium which was found to contain features similar to cold fronts.

In this paper, we present results from temperature maps of an ensemble of clusters that form within a cosmological simulation, already shown to reproduce the observed X-ray scaling relations at low redshift (Muanwong et al. 2002). This way, we are able to assess directly the range of substructure present in the cluster population. In common with observations, we see significant temperature fluctuations in the hot gas, even when there is little information present in the surface brightness distribution. In particular, we discuss the presence of a cold front in one of our bimodal clusters, which has properties consistent with the cold front in Abell 2142 (Markevitch et al. 2000).

★E-mail: lonuora@pact.cpes.susx.ac.uk

2 THE SIMULATIONS

Simulation data were generated using a parallel version of the HYDRA N-body/hydrodynamics code (Couchman, Thomas & Pearce 1995; Pearce & Couchman 1997) on the Cray T3E supercomputer at the Edinburgh Parallel Computing Centre. Full details of the simulations have already been presented elsewhere (Muanwong et al. 2002, hereafter M2002; Thomas et al. 2002), so we summarize pertinent details only.

Results are presented for a flat, low-density cosmology ($\Omega_0 = 0.35$, $\Omega_\Lambda = 0.65$, $h = 0.71$, $\sigma_8 = 0.9$), using 160^3 each of gas and dark matter particles within a box of comoving length $100\,h^{-1}$ Mpc. We consider two models: the *Radiative* model, which includes radiative cooling of the gas; and the *Preheating* model for which we additionally pre-heat the gas by raising its specific thermal energy by 1.5 keV per particle at $z = 4$. This additional energy injected into the gas increased the core entropy of clusters by approximately $100\,h^{-\frac{1}{2}}$ keV cm^2 (M2002). In both models, we adopted a time-dependent global metallicity, $Z = 0.3(t/t_0)\,Z_\odot$, where $t_0 \sim 13$ Gyr is the current age of the universe. As discussed in M2002, both models reproduce the X-ray cluster scaling relations, although the *Radiative* model contains a significantly higher cooled fraction than the *Preheating* model (15 per cent, as opposed to $\sim$0.5 per cent). In the former model, cooling is limited by numerical resolution and the cooled gas fraction is 50–100 per cent larger than that determined by Balogh et al. (2001), using results from the 2MASS and 2dF galaxy surveys (Cole et al. 2001).

Simulated cluster catalogues were produced using the same method as described in M2002. In summary, clusters were identified as clumps of particles within spheres of average overdensities compared with the comoving critical density, centred on the position of the densest dark matter particle. For this paper, we adopt an overdensity of 1000; the associated radius, R_{1000}, is approximately half the size of the virial radius, and is comparable to the extent currently probed by *Chandra*.

3 THE TEMPERATURE AND SURFACE BRIGHTNESS MAPS

Maps of emission-weighted temperature were made for each of the nine most massive clusters ($M_{1000} = 1$–$4 \times 10^{14}\ h^{-1}\ \mathrm{M}_\odot$) in the *Preheating* catalogue, and for the corresponding clusters in the *Radiative* catalogue. Each map was produced by first locating all hot ($T > 10^5$ K) gas particles within a cube of length $2R_{1000}$ along each side, centred on the cluster of interest. The length of the region along the line of sight was extended to about twice the virial radius of the cluster to include any surrounding substructure. The desired quantity was then smoothed on to a 3D array and projected along the line of sight using the SPH interpolation method (e.g. da Silva et al. 2000):

$$A(\boldsymbol{x}_j) = \frac{\sum_\alpha \sum_i A_i w_i \mathcal{W}(\Delta r_{ij}, h_i)}{\sum_\alpha \sum_i w_i \mathcal{W}(\Delta r_{ij}, h_i)}, \tag{1}$$

where

$$\mathcal{W}(\Delta r_{ij}, h_i) = \frac{W(\Delta r_{ij}, h_i)}{\sum_k W(\Delta r_{ik}, h_i)}. \tag{2}$$

The sums i extend over all particles, k over all voxels and α along the line of sight. A_i is the value of the quantity for particle i at position $\boldsymbol{r}_i$, $\boldsymbol{r}_j$ is the centroid position of voxel j, $\Delta r_{ij} = |\boldsymbol{r}_j - \boldsymbol{r}_i|$, $\boldsymbol{x}_j$ is the projected position of voxel j, w_i is a weight factor, $W(\Delta r, h)$ is the same SPH smoothing kernel used by HYDRA (Thomas & Couchman 1992) and h_i is the smoothing length of particle i ($W \to 0$ as $\Delta r \to 2h$). Equation (2) normalizes the contribution of each particle to be A_i when summed over all voxels. For mass-weighted quantities, $w_i = m_i$, and for emission-weighted quantities, $w_i = m_i n_i \Lambda(T_i, Z)$, for particle i with mass m_i, density n_i, temperature T_i and X-ray emissivity $\epsilon_i = n_i^2 \Lambda(T_i, Z)$; the cooling function, $\Lambda(T, Z)$, is the same function adopted for our simulations, using tables published by Sutherland & Dopita (1993). The smoothed distribution was projected on to a 64×64 grid, with the width of each pixel being approximately 10–20 h^{-1} kpc, smaller than the gravitational softening length used in the simulations ($25\,h^{-1}$ kpc).

Figs 1 and 2 show the emission-weighted temperature maps (with superimposed X-ray surface brightness contours and projected velocity vectors) for the *Preheating* and *Radiative* runs respectively. Surface brightness contours are normalized to the maximum value, with contour spacing in logarithmic intervals of 0.25. Velocities (in km s^{-1}) are also emission-weighted and the length of each vector represents the velocity perpendicular to the line of sight of the gas at that point.

Positive temperature fluctuations of up to three times the average, associated with compression of the gas, are evident. There also exist bright clumps of cool gas, with temperatures less than half the mean value. These features are far more abundant in the *Radiative* maps than in the *Preheating* maps because the energy injection in the *Preheating* run was large enough to erase a significant amount of substructure.

Among the nine clusters, several show clear bimodal structure (clusters 1, 2 and 8). This is most clear for the second and eighth maps, in each of which two cold clumps appear to be moving away from one another. The eighth cluster shows evidence of a sharp boundary at the leading edge of the cold clump in the upper right quadrant; when the maps for this cluster are recentred to show the cold clump in the lower right of the map, a similar sharp edge can be seen. These features are indicative of observed cold fronts and this is investigated in the next section.

The velocity vectors superimposed on the cluster maps show clear evidence for rotation in some cases (for example maps 3, 5 and 9). Ritchie & Thomas (2002) found similar rotation of the velocity field in their simulated off-centre merger of two equal-mass clusters. The contours show various degrees of ellipticity, again as found for merging clusters. The spiral patterns seen in some of the temperature maps (e.g. 3 and 5) may be due to heating by shocks produced during the merger as was seen in the simulations of Ritchie & Thomas during the interaction of cluster cores. With its relatively rounder surface brightness contours, cluster 9 may be in a later, more relaxed state.

The centres of all clusters show a decline in temperature. This is in contrast to the simulated temperature maps of Loken et al. (2002), produced using an adaptive mesh-refinement code, where the radial temperature profiles continue to rise at small radii. The Santa Barbara cluster comparison project (Frenk et al. 1999) found the general result that for non-radiative gas, SPH codes produce a central flat or slightly declining temperature profile, while all of the grid codes produce a temperature profile that continues to rise to the resolution limit. This conflict between results using the different codes still needs to be resolved. Springel & Hernquist (2002) recently discussed entropy conservation problems in SPH simulations. In our simulations, however, the entropy fluctuations induced by pre-heating and radiative cooling are far larger than numerical effects.

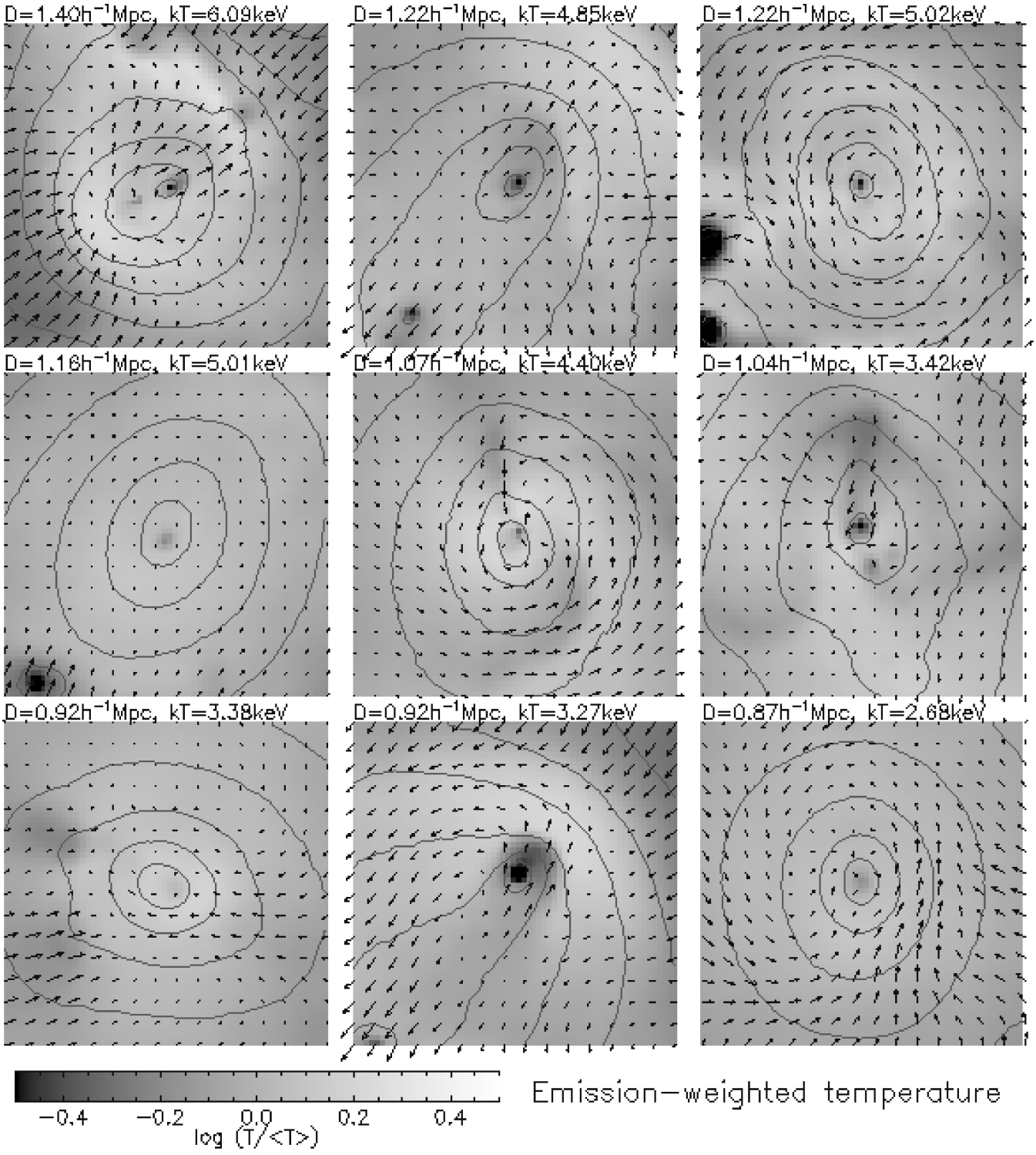

Figure 1. Temperature maps of the nine largest clusters in the *Preheating* run with surface brightness contours and velocity vectors overlaid. We label the clusters 1–9 in order of virial temperature, starting from the top-left and reading across then down. Given above each panel is the size across the region ($2R_{1000}$) and the emission-weighted temperature when averaged over all hot gas within R_{1000}. This figure is available in colour in the online version of the journal on *Synergy*.

Fabian (2002) noted that all of the cores mapped so far by *Chandra* with radiative cooling times of a few billion years show significant central temperature drops. This temperature drop of a factor of about 3 or more in the central region of the clusters was explained by Fabian as possibly due to a combination of radiative cooling and gas introduced from dense cooling subclusters, as we see here.

We present circularly averaged emission-weighted temperature profiles for the *Radiative* maps in Fig. 3. The more regular of our

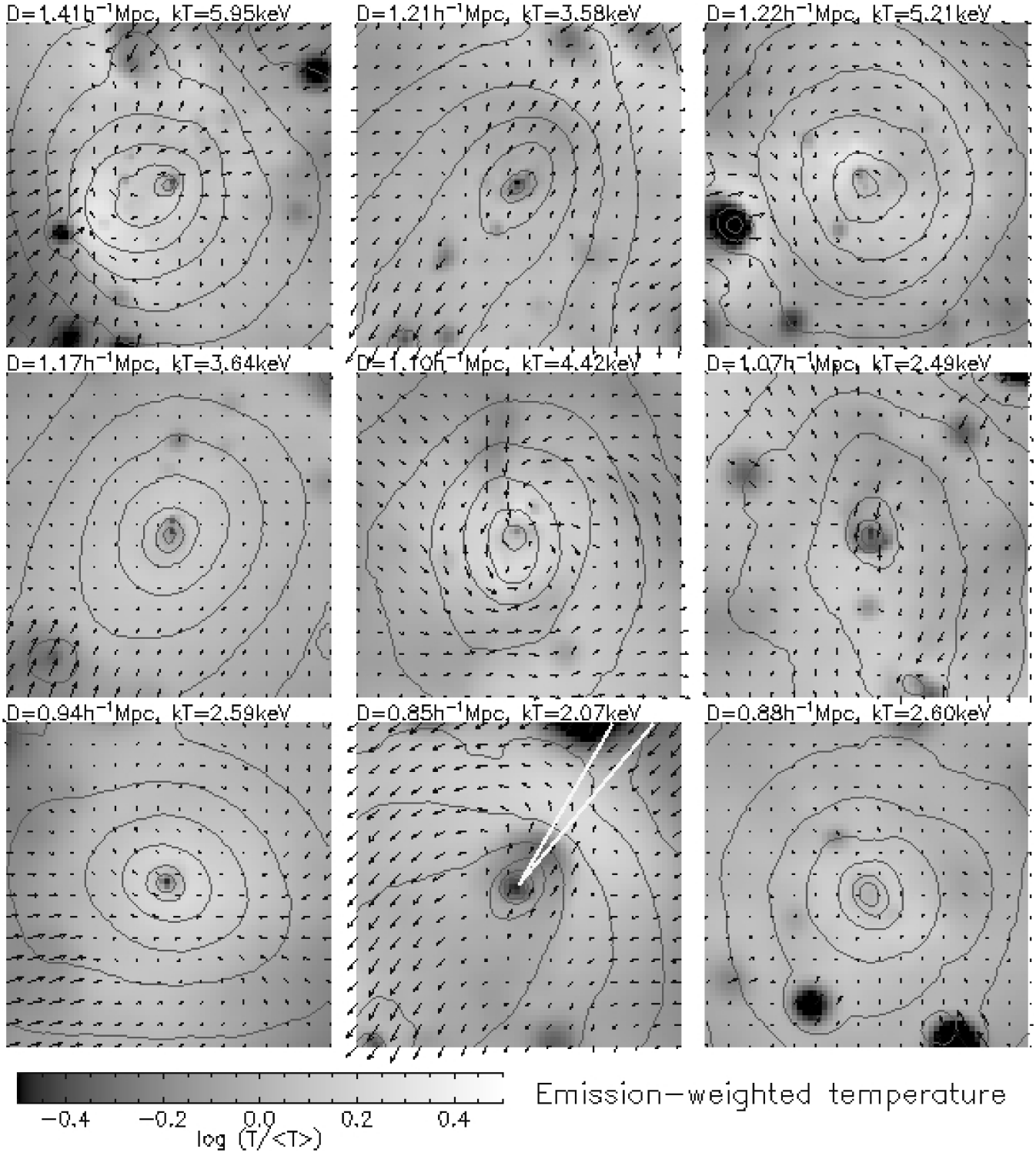

Figure 2. Temperature maps for the *Radiative* run for the same clusters as in Fig. 1. The slice marked in map 8 corresponds to the region used to illustrate the presence of a cold front, as discussed in Section 4. This figure is available in colour in the online version of the journal on *Synergy*.

clusters (4, 7 and 9) exhibit the type of gradually declining temperature profile found by Loken et al. (2002) for those clusters in their sample that appeared to be regular and symmetric. Loken et al. noted that even the temperature profiles of the non-symmetric, irregular clusters in their sample did not depart greatly from the general appearance, but with bumps or wiggles appearing corresponding to merging subclusters. The other clusters in our samples, however, exhibit a variety of profiles with the irregular clusters (2 and 6) even appearing approximately isothermal when circularly averaged. It therefore seems that a universal temperature profile can only be applied to a very limited number of clusters which appear very regular and symmetric, at least in the inner regions ($R < R_{1000}$).

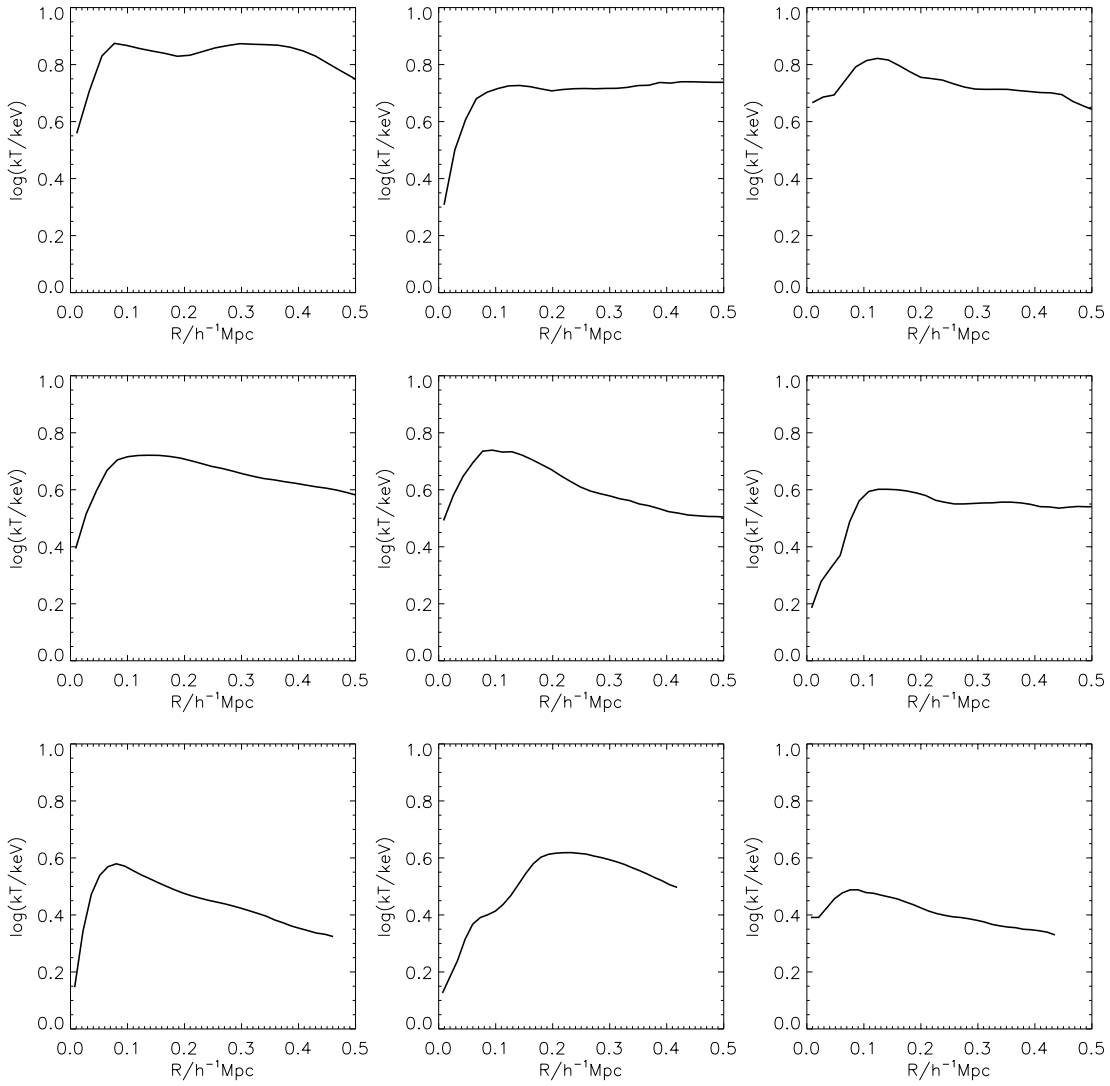

Figure 3. Circularly averaged temperature profiles for the *Radiative* maps.

4 IDENTIFICATION OF A POSSIBLE COLD FRONT IN MAP 8

Of the nine cluster maps produced here, map 8 appeared to have the strongest visual evidence for the presence of cold fronts. To investigate whether the physical properties are consistent with a cold front, profiles were produced of emission-weighted temperature, X-ray surface brightness, pressure and density across the surface brightness and temperature discontinuity in the upper right quadrant of the *Radiative* map (Fig. 2). Pixels with position angles between 30° and 40° with respect to the image centre were binned as a function of radius for each of the four parameters. The profiles are shown in Fig. 4.

A sharp rise in temperature by a factor of about 3 over a radial distance of $<0.1\ h^{-1}$ Mpc was found; comparison with the observed temperature profile across the north-western edge of the X-ray image for Abell 2142 in Markevitch et al. (2000) shows that the radial scale is very similar and the temperature increases by approximately the same factor. In the region of the cold front, the pressure profile of the simulated cluster was smooth and fairly flat, falling off at larger radius. For the pressure profile to flatten in this region, where the temperature is rising sharply, implies that the gas density must be dropping sharply, again similar to the profile in Markevitch et al. (2000). The relative radial velocity across the cold front is approximately 150 km s^{-1}, implying that the cold clump is moving subsonically at around half the local sound speed.

Similar profiles, consistent with cold fronts, were found when the binning was repeated across the surface brightness edge in the lower left quadrant, and also for the *Preheating* run for the same cluster. The overall picture for this cluster, taking into account also the direction of the velocity vectors, is of two cold subclumps moving away from each other, which fits in with the merger scenario suggested by Markevitch et al. (2000) of subclumps falling in along filaments. The cold, low-entropy cores are undisrupted by the merger and continue on through the cluster.

5 DISCUSSION

Temperature maps of the nine largest clusters in the simulated cluster catalogues of M2002 show clearly that the clusters do contain substructure. Features that are seen include cold clumps,

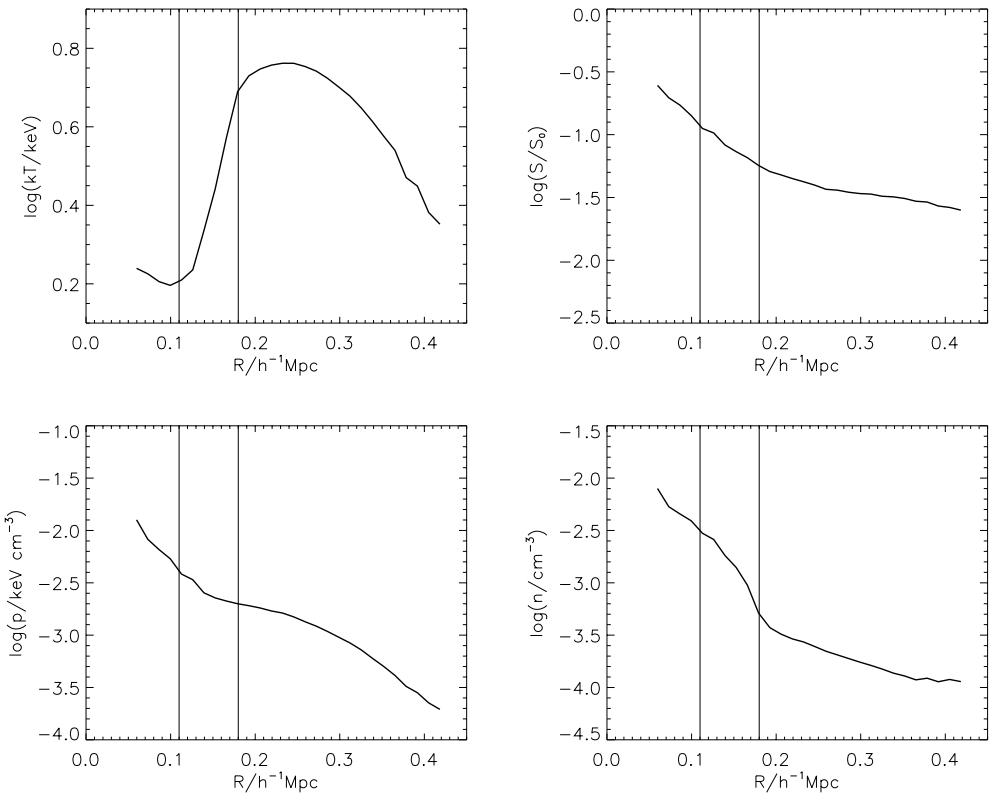

Figure 4. Emission-weighted profiles of temperature, X-ray surface brightness (normalized to the maximum value), pressure and density across the cold front in cluster 8 in the *Radiative* simulation. The vertical lines are included to illustrate the cold-front region. This figure is available in colour in the online version of the journal on *Synergy*.

some of which may be consistent with the infall of cold subclusters, hot spiral features consistent with shocks produced in mergers, and at least one map containing cold fronts. Elliptical surface brightness contours are the norm, and rotation, as expected in off-centre mergers, is common. The *Preheating* maps appear 'cleaner', with fewer cold clumps present than for the *Radiative* maps, since the gas has been heated at $z = 4$, wiping out many of the colder blobs. The remaining cold clumps seen in these maps did seem to be associated with motion into or through the cluster.

In this paper our main aim has been to demonstrate that simulated maps contain a variety of substructure. Overall the hot substructure seems similar in the two models studied, but the *Radiative* model can be distinguished from the *Preheating* model by the number of cold blobs. High-resolution temperature maps from *Chandra* will provide a test of models of the thermal history of the intracluster medium. Our future work will focus on the evolution of structure in clusters and on a larger range of cluster masses extending down to the size of groups.

ACKNOWLEDGMENTS

We thank the anonymous referee for suggestions that have improved the quality of this paper. The simulations used in this paper were carried out on the Cray T3E at the Edinburgh Parallel Computing Centre as part of the Virgo Consortium programme of investigations into the formation of structure in the Universe. LIO was supported in part by the Leverhulme Trust and STK by PPARC; PAT is a PPARC Lecturer Fellow.

REFERENCES

Balogh M. L., Pearce F. R., Bower R. G., Kay S. T., 2001, MNRAS, 326, 1228
Bialek J. J., Evrard A. E., Mohr J. J., 2002, ApJ, 578, L9
Briel U. G., Henry J. P., 1994, Nat, 372, 439
Cole S. et al., 2001, MNRAS, 326, 255
Couchman H. M. P., Thomas P. A., Pearce F. R., 1995, ApJ, 452, 797
da Silva A. C., Barbosa D., Liddle A. R., Thomas P. A., 2000, MNRAS, 317, 37
Evrard A. E., Mohr J. J., Fabricant D. G., Geller M. J., 1993, ApJ, 419, L9
Fabian A. C., 2002, in Gilfanov M. et al. eds, Proceedings of the MPA/ESO Conference. Light houses of the Universe: The Most Luminous Celestial Objects and their use for Cosmology. Springer-Verlag, Berlin, p. 24
Forman W., Jones C., Markevitch M., Vikhlinin A., Churazov E., 2001, in Neumann D. M., Van J. T. T., eds, XXIst Moriond Astrophysics Meeting. Clusters of Galaxies and the High Redshift Universe Observed in X-rays. Recent results of XMM-Newton and Chandra
Frenk C. S. et al., 1999, ApJ, 525, 554
Loken C., Norman M. L., Nelson E., Burns J., Bryan G. L., Motl P., 2002, ApJ, 579, 571
Markevitch M., 1996, ApJ, 465, L1
Markevitch M., Vikhlinin A., 2001, ApJ, 563, 95
Markevitch M. et al., 2000, ApJ, 541, 542
Markevitch M., Gonzalez A. H., David L., Vikhlinin A., Murray S., Forman W., Jones C., Tucker W., 2002, ApJ, 567, 27
Mazzotta P., Fusco-Femiano R., Vikhlinin A., 2002, ApJ, 569, L31
Mohr J. J., Fabricant D. G., Geller M. J., 1993, ApJ, 413, 492
Mohr J. J., Evrard A. E., Fabricant D. G., Geller M. J., 1995, ApJ, 447, 8
Muanwong O., Thomas P. A., Kay S. T., Pearce F. R., 2002, MNRAS, 336, 527 (M2002)
Nagai D., Kravtsov A. V., 2003, astro-ph/0206469

Pearce F. R., Couchman H. M. P., 1997, New Astron., 2, 411
Pearce F. R., Thomas P. A., Couchman H. M. P., 1994, MNRAS, 268, 953
Ricker P. M., Sarazin C. L., 2001, ApJ, 561, 621
Ritchie B., Thomas P. A., 2002, MNRAS, 329, 675
Roettiger K., Burns J. O., Loken C., 1993, ApJ, 407, L53
Roettiger K., Loken C., Burns J. O., 1997, ApJS, 109, 307
Schindler S., Müller E., 1993, A&A, 272, 137
Springel V., Hernquist L., 2002, MNRAS, 333, 649
Sutherland R. S., Dopita M. A., 1993, ApJS, 88, 253
Takizawa M., 1999, ApJ, 520, 514
Takizawa M., 2000, ApJ, 532, 183
Thomas P. A., Couchman H. M. P., 1992, MNRAS, 257, 11
Thomas P. A., Muanwong O., Kay S. T., Liddle A. R., 2002, MNRAS, 330, L48
Vikhlinin A., Markevitch M., Murray S. S., 2001, ApJ, 551, 160

This paper has been typeset from a TEX/LATEX file prepared by the author.